Electronic Supplementary Material (ESI) for Materials Chemistry Frontiers.
This journal is © the Partner Organisations 2020

# Electronic Supporting Information

# AIEgen based Polymorphs with Solvent Regulated Crystal-to-Crystal Switch

Liming Lai[a], Bing Fang[a], Wenyu Cheng[a], Pengyu Li[a], Yantu Zhang[b] and Meizhen Yin*[a]

[a] State Key Laboratory of Chemical Resource Engineering, Beijing Advanced Innovation Center for Soft Matter Science and Engineering, Beijing Laboratory of Biomedical Materials, Beijing University of Chemical Technology, Beijing 100029, P. R. China.*E-mail: yinmz@mail.buct.edu.cn

[b] College of Chemistry and Chemical Engineering, Yan'an University, Yan'an, Shanxi Province 716000, P. R. China.

## Experimental Section

### Materials:

9H-carbazole, 2,7-dibromo-9-fluorenone, Bis (tri-tert-butyl phosphine) palladium potassium carbonate, are purchased from Alfa Aesar Co. and use without further purification. Dichloromethane and n-Hexane were dried by calcium hydroxide overnight and then distilled under reduced pressure before use. All solvents were dried prior to use with appropriate drying agents. Column chromatography was performed using silica gel 60 (300-400 mesh). Analytical thin layer chromatography was carried

out on Yantai chemical industry silica gel plates and visualized by UV lamp.

**Instrumentation:**

$^{1}$H-NMR spectra are recorded on a Bruker 400 (400 MHz) spectrometer in deuterated $CDCl_3$ using tetramethylsilane (TMS; h = 0) as internal reference. HR-MS were measured with a XEVO-G2QTOF (ESI) (USA). Fluorescence spectroscopic studies are performed on a fluorescence spectrophotometer (Horiba Jobin Yvon FluoroMax-4 NIR, NJ, USA). UV–vis spectra are obtained on a spectrometer (Cintra 20, GBC, Australia). 1931 CIE color coordinates were measured using a HORIBA Jobin-Yvon FluoroMax-4 spectrofluorimeter. The percentage distribution of each lifetime component to the total decay curve and photoluminescence quantum yield is recorded using an Edinburgh Instruments FLS 980 Fluorspectrophotometer. Powder X-ray diffraction (PXRD) patterns carried by a D/max2500 VB2+/PC X-ray diffractometer (Rigaku) using Cu Kα radiation in the 2θ range 5-40°. Digital photographs were taken by Canon 600D (Canon, Japan) digital cameras.

Computational details: All highest occupied molecular orbital (HOMO) and lowest unoccupied molecular orbital (LUMO) were calculated by density functional theory (DFT) calculations carried out by using B3LYP/6-31g (d) within the Gaussian 09 suite. The aggregation effect was considered by using ONIOM method with QM and MM layers in Gaussian 09 program. The UFF force field was used with the restrained electrostatic potential (RESP) partial charges for the MM treatment. And the computation model for crystal was built by digging a cluster from the X-ray crystal structures. All calculations of geometry optimizations for the ground state ($S_0$) and the first excited state ($S_1$) of crystal phase were respectively studied by using the density

functional theory (DFT) and TD-DFT by M062X hybrid functional combined with cc-pvdz basis sets.

X-Ray Single Crystal Diffraction Analysis: Single crystal monochromatic X-ray diffraction measurements were carried out on a Bruker D8 Venture diffractometer outfitted with a PHOTON-100 complementary metal oxide semiconductor detector, using microfocus Mo Kα radiation (λ = 0.71073 Å) that was operated at 50 kV and 40 mA at 123 K by chilled nitrogen flow controlled by a KRYOFLEX II low temperature attachment. Cambridge Crystallographic Data Centre (CCDC) 1973733–1973734 contains the supplementary crystallographic data for this paper. These data can be obtained free of charge from The Cambridge Crystallographic Data Centre.

## Synthesis of Compound DCzFO:

9H-carbazole (2.5 mmol, 0.7 g), 2,7-dibromo-9-fluorenone (1.2 mmol,0.4 g), and $K_2CO_3$ (3.4 mmol,0.45 g) were dissolved in toluene (15 mL). After the flask was evacuated under vacuum and purged with dry nitrogen for 20min, Bis (tri-tert-butyl phosphine) palladium was added, followed by stirring at 120 °C for 18 h. After cooling to room temperature, the resulting mixture was poured into 200 mL of deionized water, extracted with dichloromethane (3×100 mL) and the organic layers were washed with brine, dried over anhydrous $Na_2SO_4$, and concentrated in vacuo. The crude product was purified by using column chromatography with n-Hexane/dichloromethane (v/v = 3:1) as the eluent to product orange solids (0.43 g, yield: 71.7%).$^1$H NMR (400 MHz, $CDCl_3$) δ 8.17 (d, *J* = 7.8 Hz, 4H), 7.97 (d, *J* = 1.5 Hz, 2H), 7.85 (d, *J* = 7.9 Hz, 2H), 7.78 (dd, *J* = 7.9, 1.7 Hz, 2H), 7.49-7.43 (m, 8H), 7.36-7.30 (m, 4H). $^{13}$C NMR (101

MHz, $CDCl_3$) δ 142.55 (s), 140.55 (s), 139.11 (s), 136.40 (s), 133.20 (s), 126.38 (s), 123.86 (s), 123.28 (s), 121.99 (s), 120.65 (s), 109.87 (s). ESI-TOF: $C_{37}H_{22}N_2O$, m/z calcd for $[M+H]^+$ 512.18, found, 512.4709.

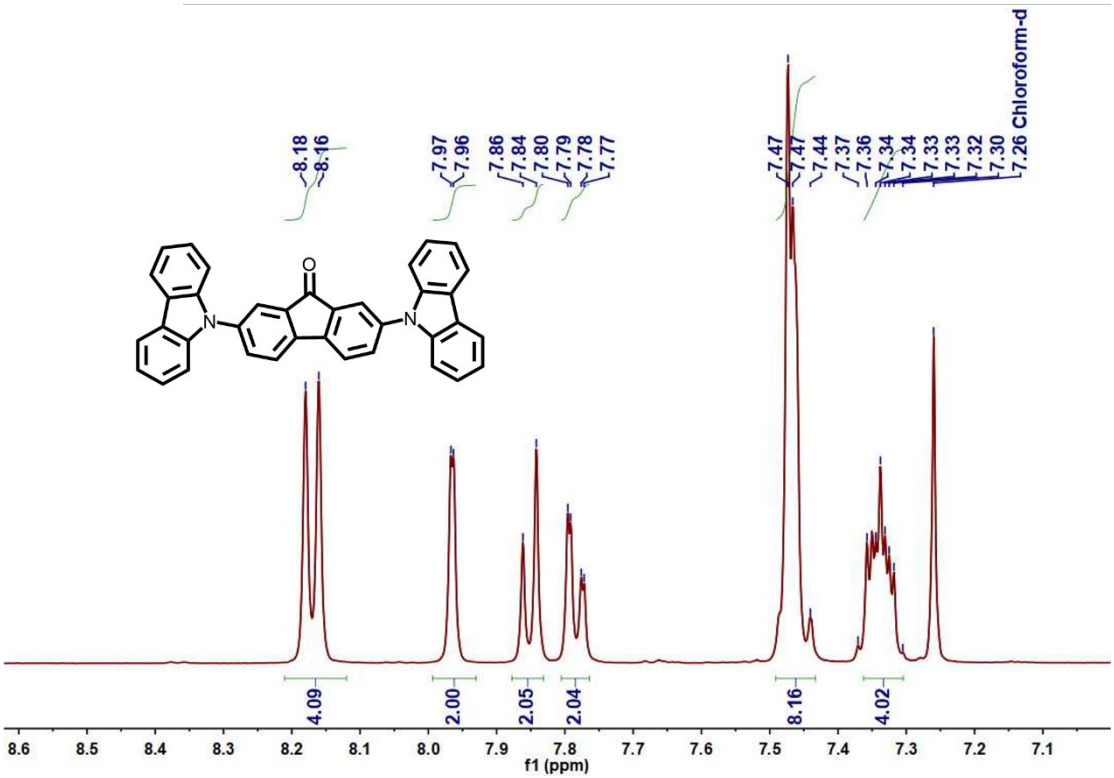


**Figure S1** $^1H$ NMR spectrum of **DCzFO** in $CDCl_3$.

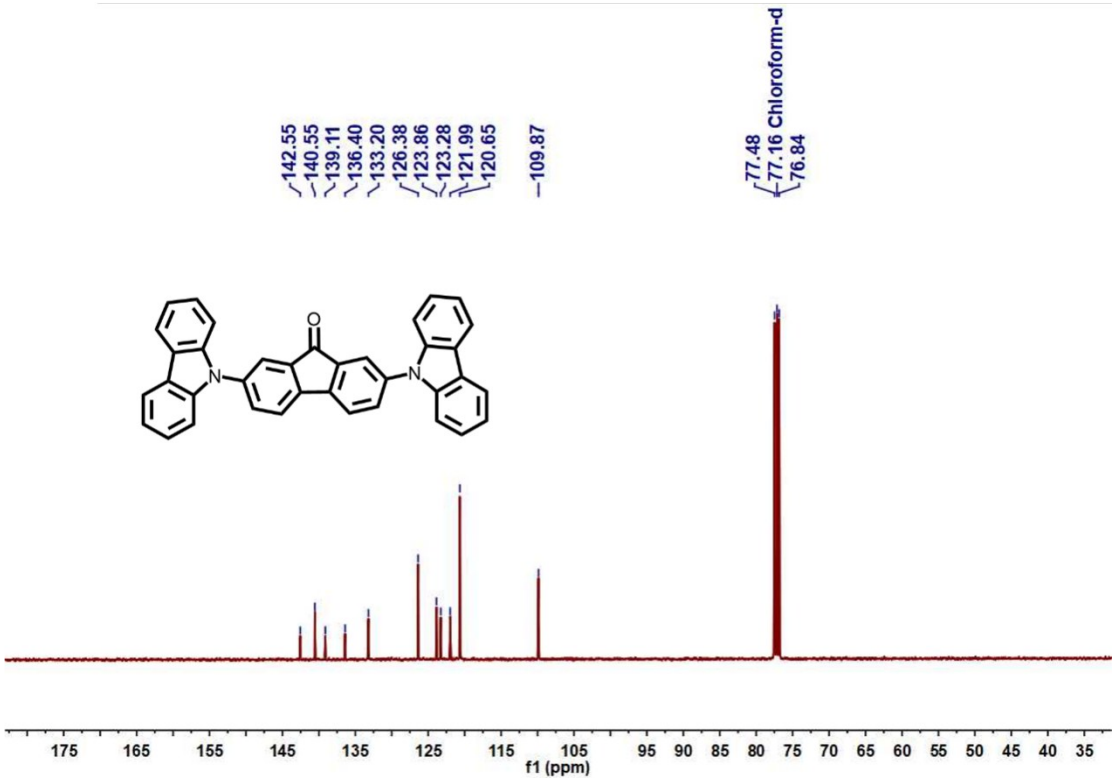


**Figure S2** $^{13}C$ NMR spectrum of **DCzFO** in $CDCl_3$.

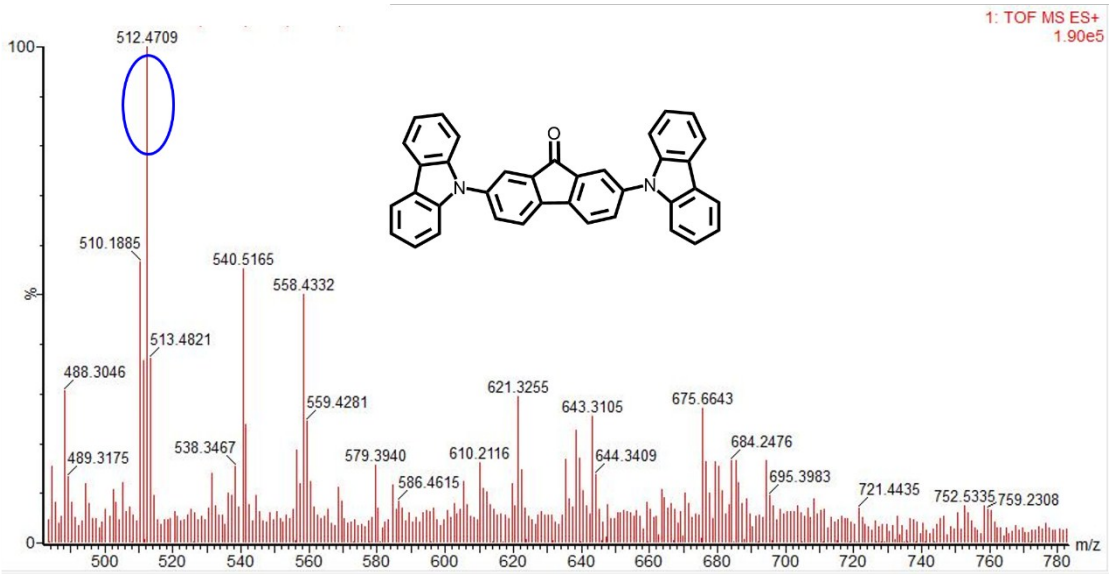


**Figure S3** ESI-TOF of **DCzFO**.

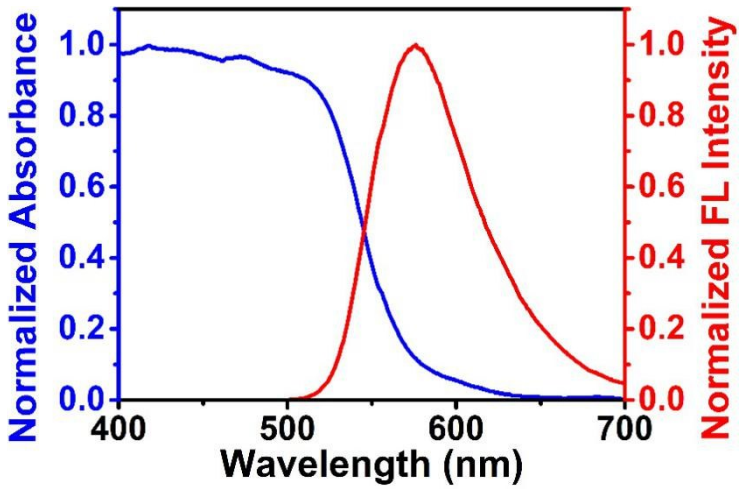


**Figure S4** Normalized UV-vis and fluorescent (FL) spectra ($\lambda_{ex}$ = 400 nm) of original powder.

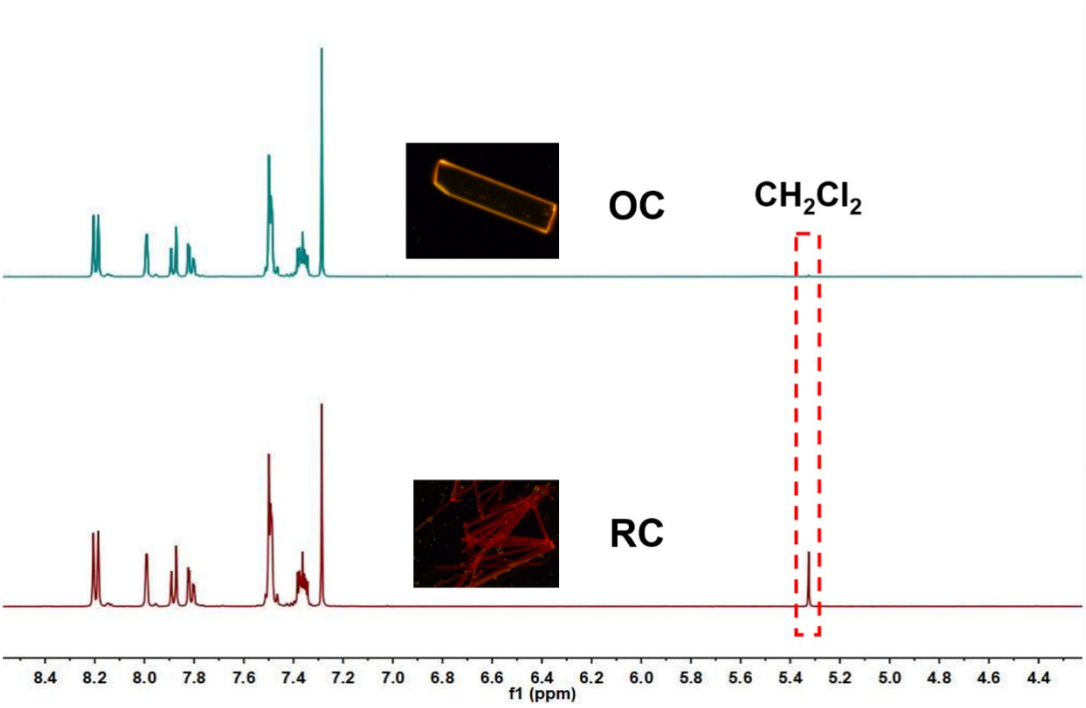


**Figure S5** $^1$H NMR spectra of **OC** and **RC**.

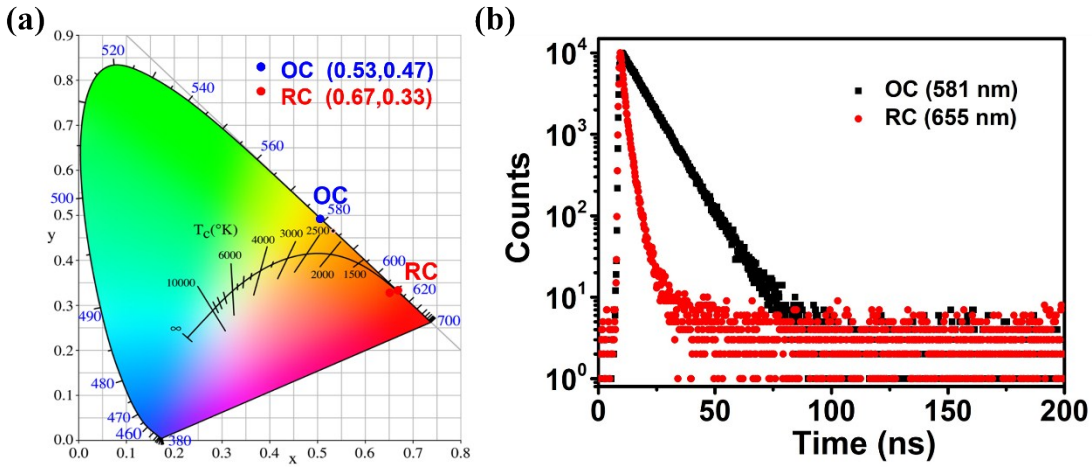


**Figure S6** (a) CIE coordinate diagram for **OC** and **RC**. (b) Transient decay spectra of **OC** and **RC**.

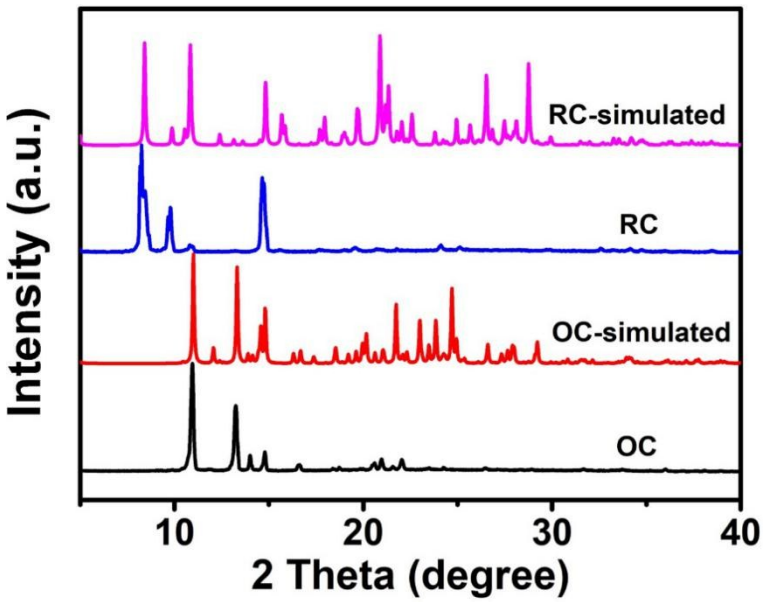


**Figure S7** Powder X-ray diffraction of **OC**, **RC** and the simulated pattern based on signal crystal data.

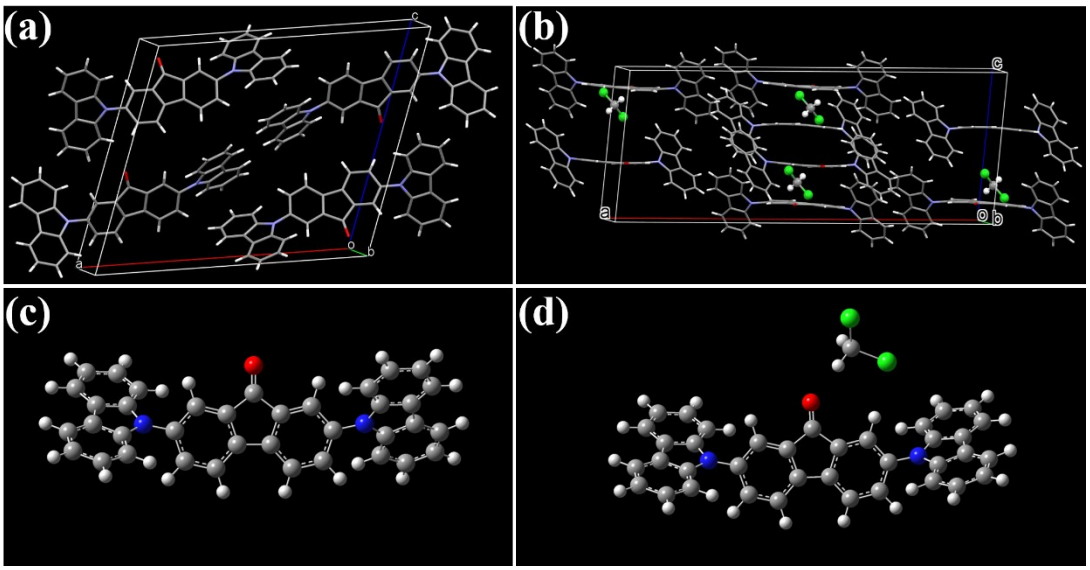


**Figure S8** Unit cell of (a) **OC** and (b) **RC**. Crystal structure of (c) **OC** and (d) **RC**.

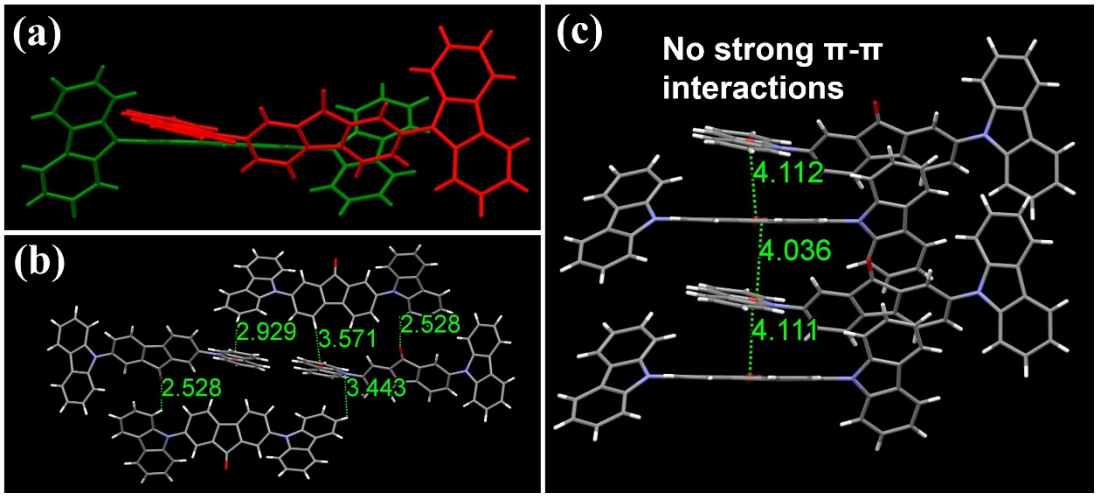


**Figure S9** No obvious π-π interaction is observed in **OC**. (a) Overlap between adjacent molecules. (b) Loose 3-dimension net structure. (c) Weak π-π interactions . Interaction distances (dashed lines) are in Å.

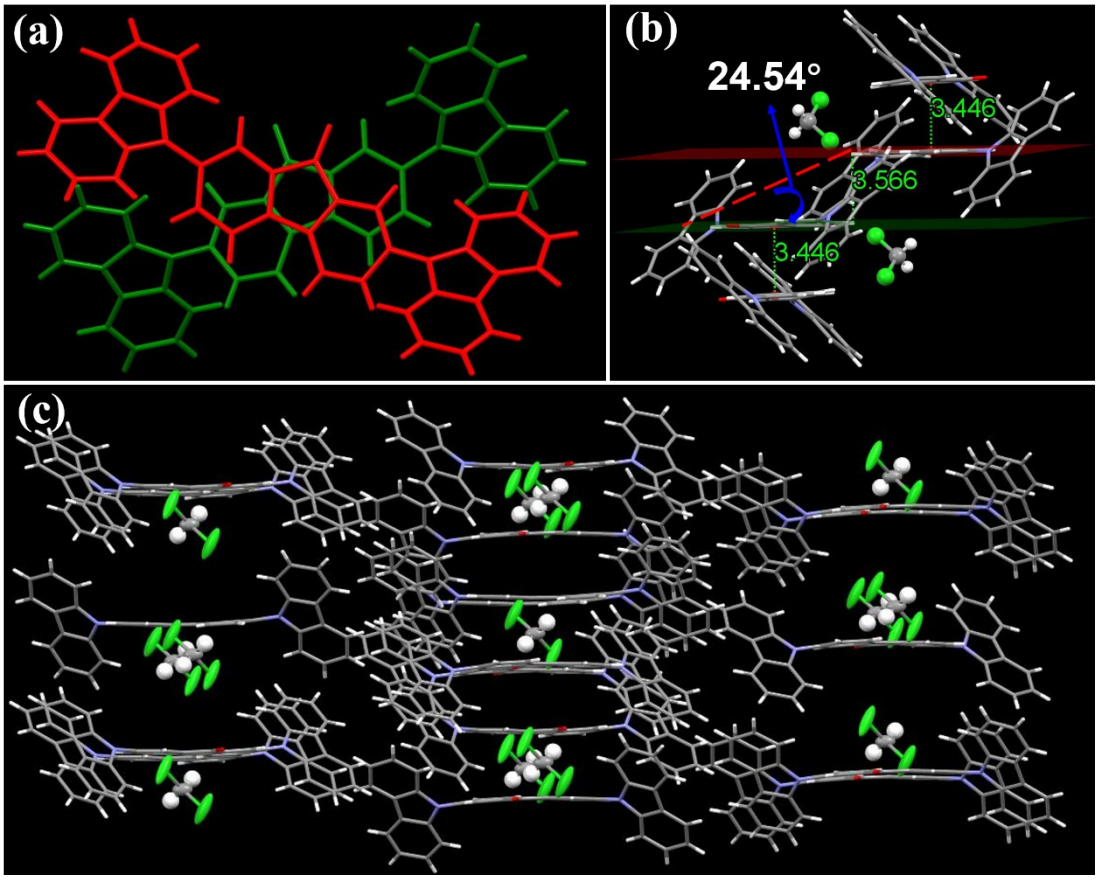


**Figure S10** (a) Obvious molecular overlap and π-π stacking mode in **RC**. (b) Two adjacent dimers and strong π-π interactions of **RC**. (c) Compact 3-dimension net structure of **RC**.

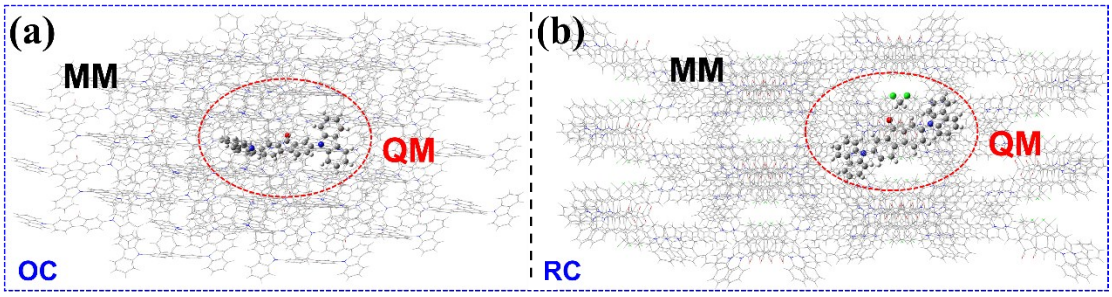


**Figure S11** QM/MM model of **DCzFO** for (a) **OC** and (b) **RC**. The central one is treated as QM part and the surrounding ones act as the MM parts. In the geometry optimization, the QM part is active and the MM part is frozen.

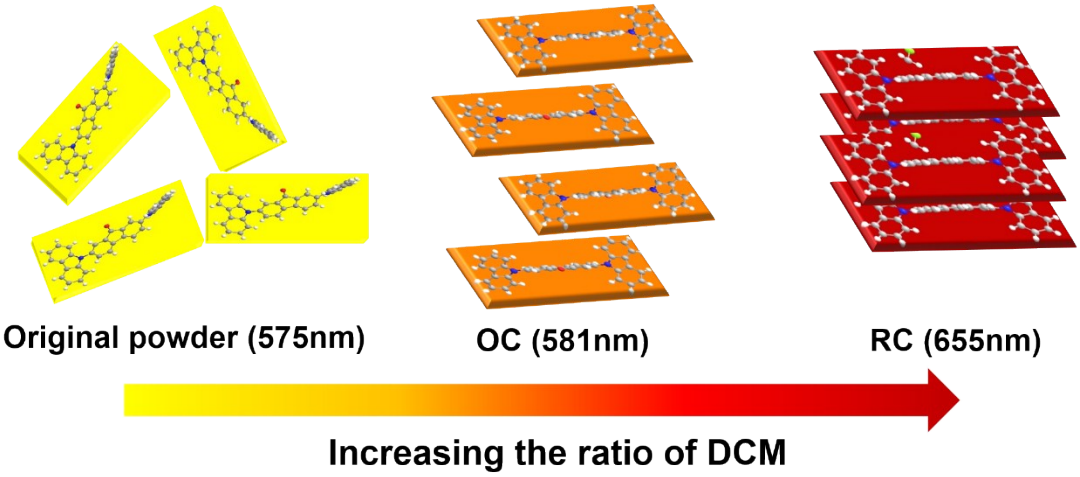


**Figure S12** Schematic diagram of the molecular conformations, arrangements of **DCzFO** and their corresponding emission colors.

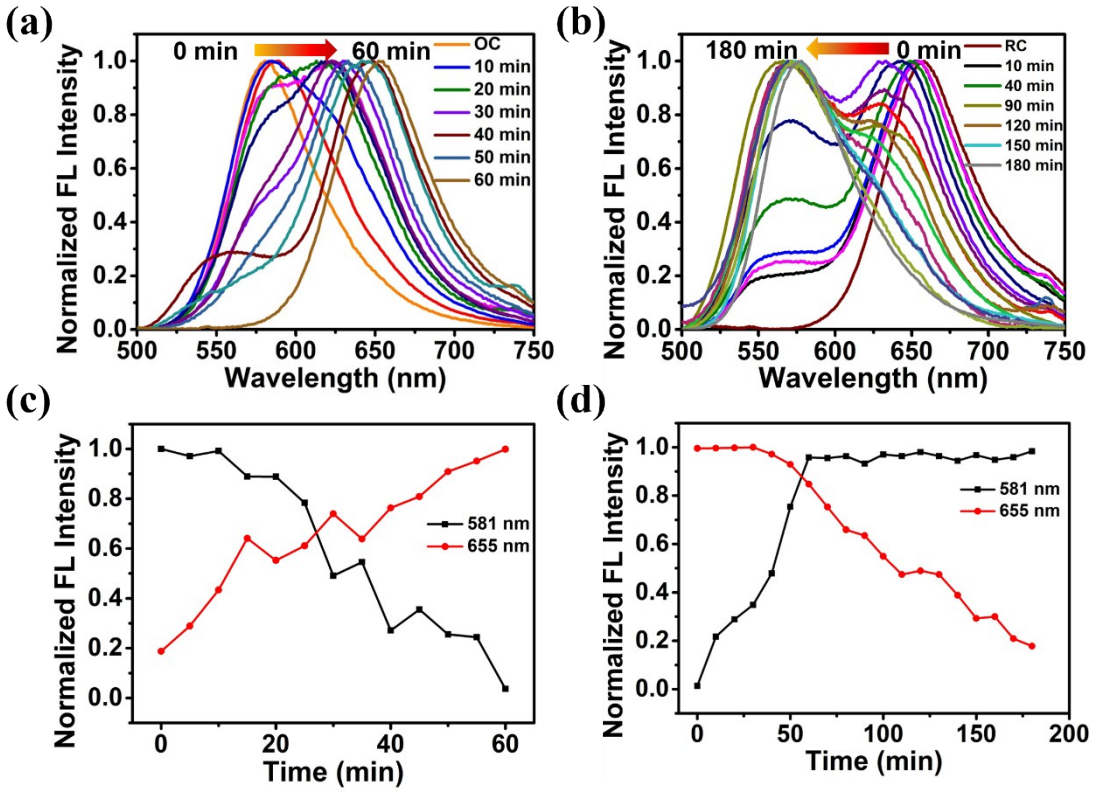


**Figure S13** (a) Normalized FL spectra of **OC** at various fuming time every 10 minutes from 0 to 60 min. (b) Normalized FL spectra of **RC** at various fuming time every 10 minutes from 0 to 180 min. Normalized FL intensity of **OC** (c) and **RC**(d) located at 581 nm and 655 nm versus fuming time. $\lambda_{ex}$ : 400 nm.

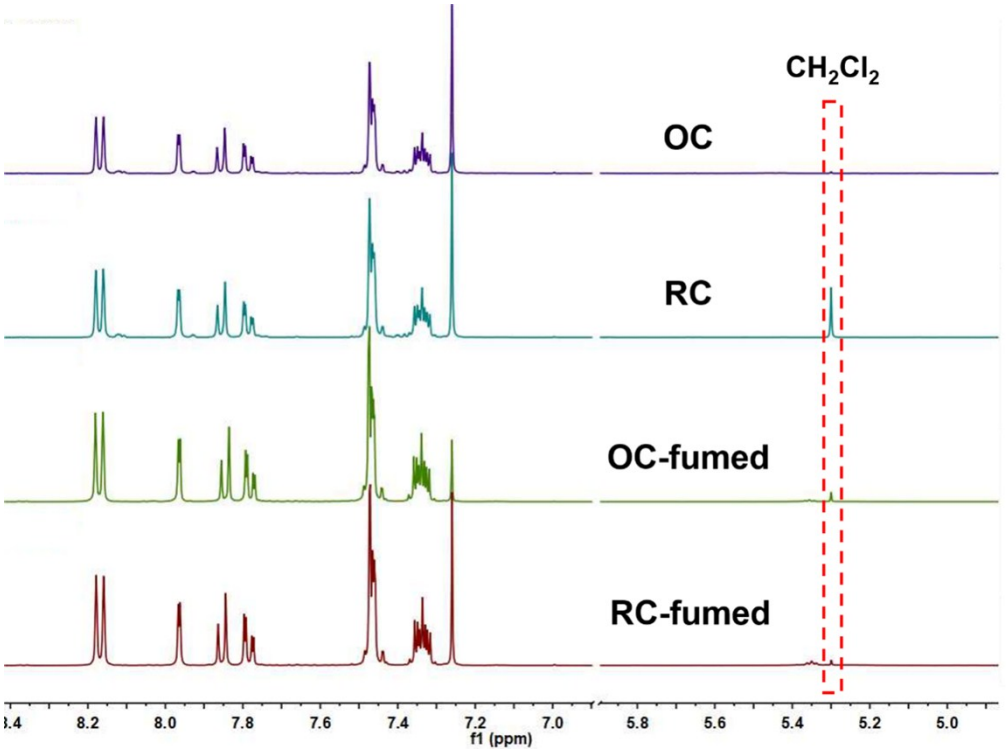


**Figure S14** $^{1}$H NMR spectra of **OC** and **RC** sample before and after vapor fumed with DCM and n-hexane in $CDCl_3$, respectively.

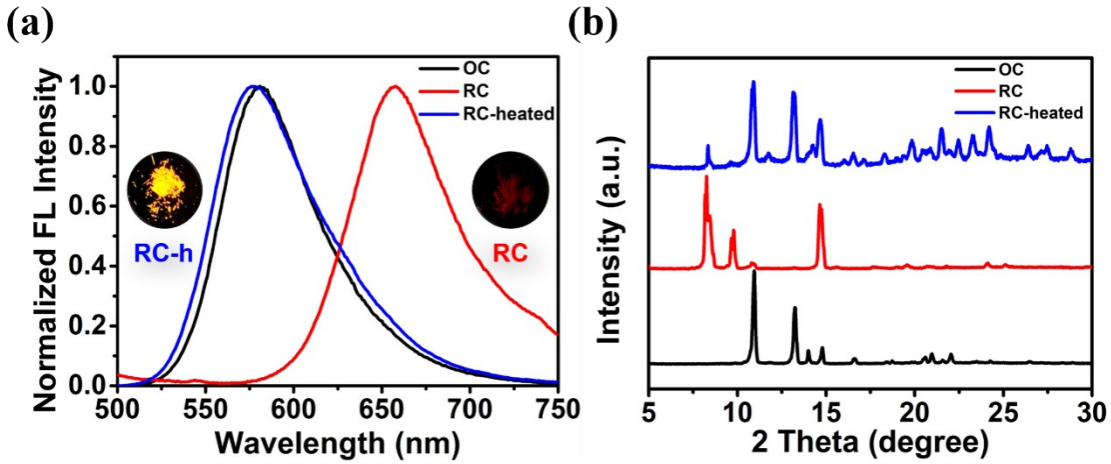


**Figure S15** (a) Normalized FL spectra ($\lambda_{ex}$ = 400 nm) and (b) powder x-ray diffraction of **OC**, **RC** and **RC-heated** samples.

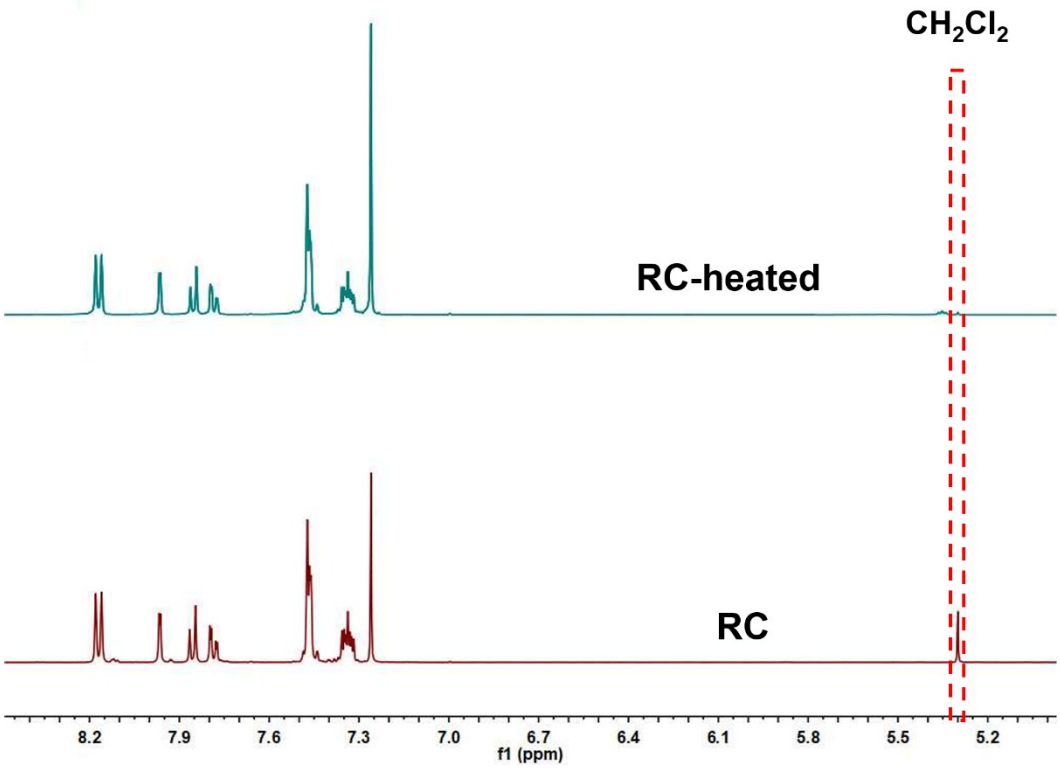


**Figure S16** $^{1}$H NMR spectra of **RC** sample before and after heated in $CDCl_3$.

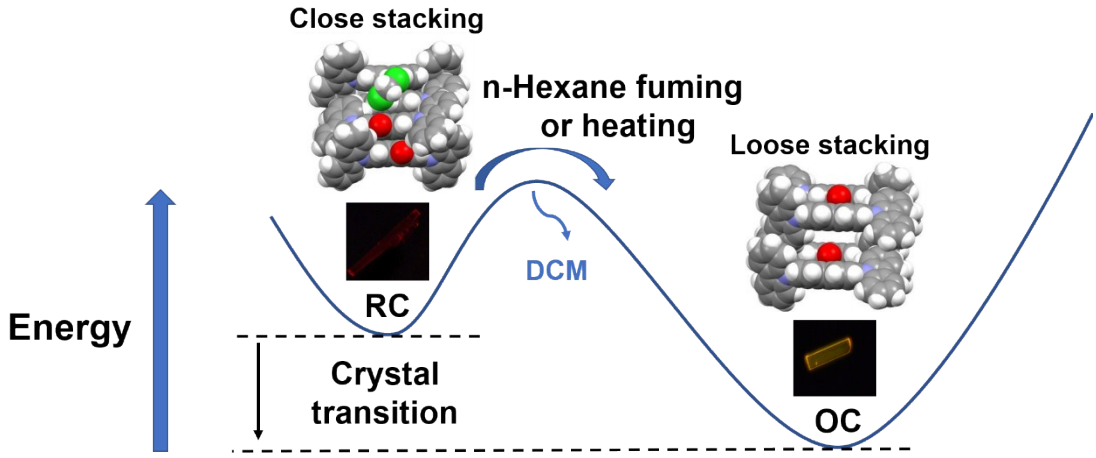


**Figure S17** Diagram of the energies for **OC** and **RC**.

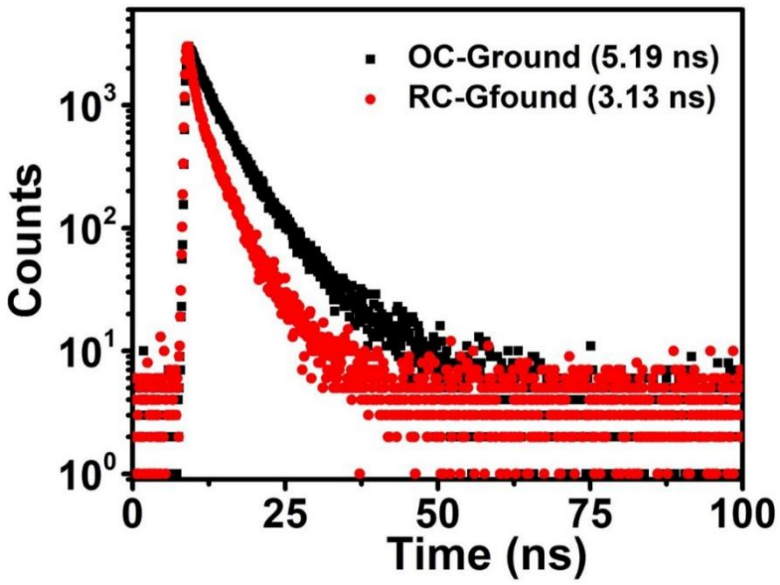


**Figure S18** Transient decay spectra of **OC-G** and **RC-G** samples.

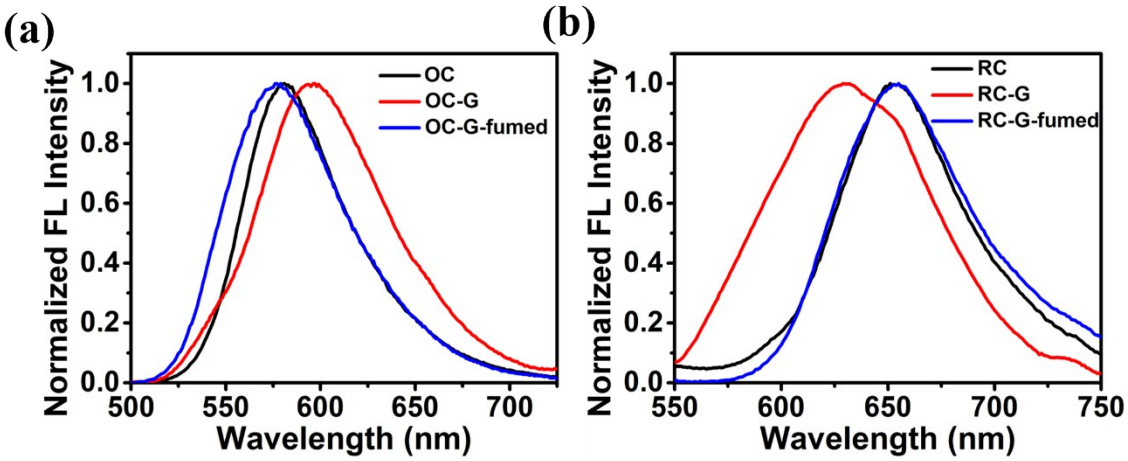


**Figure S19** Normalized FL spectra of sample **OC-G** (a) before and after n-Hexane vapor fuming and **RC-G** (b) before and after DCM vapor fuming. ($\lambda_{ex}$ = 400 nm)

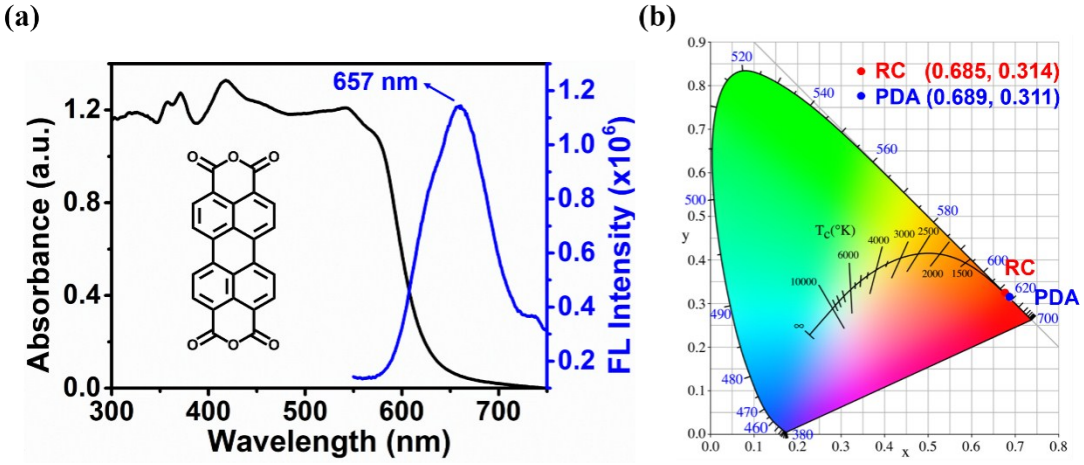


**Figure S20** a) Normalized UV-vis and FL spectra ($\lambda_{ex}$ = 400 nm) of compound 3,4,9,10-Perylenetetracarboxylic dianhydride (PDA). b) The CIE coordinate diagram for **RC** and PDA.

**Table S1.** Calculated results for OC and RC based on crystal data.

| Crystal form | HOMO (eV) | LUMO (eV) | $\Delta E_g$ (eV) | Dipole Moment (Debye) |
|---|---|---|---|---|
| **OC** | -2.59 | -2.78 | 2.81 | 3.51 |
| **RC** | -5.40 | -5.42 | 2.64 | 5.66 |

**Table S2.** The photophysical parameters including Emission maxima ($\lambda_{FL}$), quantum yields ($\Phi_F$), fluorescence lifetimes ($\tau_{FL}$), radiative rates ($k_r$), and non-radiative rates ($k_{nr}$) of **OC**, **RC**, **OC-G**, and **RC-G** sample. $k_r = \Phi_F/\tau_{FL}$; $k_{nr} = (1-\Phi_F)/\tau_{FL}$.

| Simple | $\lambda_{FL}$ (nm) | $\tau_F$ (ns) | $\Phi_F$ (%) | $k_r$ ($10^7$ $s^{-1}$) | $k_{nr}$ ($10^7$ $s^{-1}$) |
|---|---|---|---|---|---|
| **OC** | 581 | 8.85 | 19.29 | 2.2 | 9.1 |
| **RC** | 655 | 1.73 | 4.26 | 2.5 | 55 |
| **OC-G** | 597 | 5.19 | 4.97 | 0.96 | 18 |
| **RC-G** | 630 | 3.13 | 9.71 | 3.1 | 29 |

**Table S3.** Crystal data for **OC** and **RC** crystals.

| Identification code | OC | RC |
|---|---|---|
| **Empirical formula** | $C_{37}H_{22}N_2O$ | $C_{37.5}H_{23}ClN_2O$ |
| **Formula weight** | 510.57 | 553.03 |
| **Temperature / K** | 111.45(10) | 111.35(10) |
| **Crystal system** | monoclinic | monoclinic |
| **Space group** | $P2_1/c$ | C2/c |
| **a / Å, b / Å, c / Å** | 19.8760(19), 7.9623(9), 17.0139(19) | 35.988(2), 10.9785(6), 13.4888(10) |
| **α/°, β/°, γ/°** | 90.00, 109.105(11), 90.00 | 90.00, 95.548(5), 90.00 |
| **Volume / Å$^3$** | 2544.3(5) | 5304.4(6) |
| **Z** | 4 | 8 |
| **$\rho_{calc}$ / mg mm$^{-3}$** | 1.333 | 1.385 |
| **μ / mm$^{-1}$** | 0.080 | 0.180 |
| **F (000)** | 1064 | 2296 |
| **Crystal size / mm$^3$** | 0.45 × 0.05 × 0.02 | 0.25 × 0.14 × 0.03 |
| **2θ range for data collection** | 6.14 to 52° | 6.06 to 52° |
| **Index ranges** | -24 ≤ h ≤ 24, -9 ≤ k ≤ 9, -20 ≤ l ≤ 20 | -44 ≤ h ≤ 44, -13 ≤ k ≤ 12, -15 ≤ l ≤ 16 |
| **Reflections collected** | 19121 | 21276 |
| **Independent reflections** | 4993[R(int) = 0.0604 (inf-0.9Å)] | 5219[R(int) = 0.0523 (inf-0.9Å)] |
| **Data/restraints/parameters** | 4993/0/361 | 5219/0/375 |
| **Goodness-of-fit on F$^2$** | 1.064 | 1.060 |
| **Final R indexes [I>2σ (I) i.e. $F_o$>4σ ($F_o$)]** | $R_1$ = 0.0505, $wR_2$ = 0.1013 | $R_1$ = 0.0879, $wR_2$ = 0.2042 |
| **Final R indexes [all data]** | $R_1$ = 0.0780, $wR_2$ = 0.1181 | $R_1$ = 0.1143, $wR_2$ = 0.2236 |
| **Largest diff. peak/hole / e Å$^{-3}$** | 0.215/-0.216 | 1.834/-1.982 |
| **Flack Parameters** | N | N |
| **Completeness** | 0.9971 | 0.9974 |